Published in final edited form as:
Sci Transl Med. 2013 June 19; 5(190): 190ra81. doi:10.1126/scitranslmed.3006276.

Silver Enhances Antibiotic Activity Against Gram-negative Bacteria

J. Ruben Morones-Ramirez[1,4], **Jonathan A. Winkler**[1,2], **Catherine S. Spina**[3,4], and **James J. Collins**[1,2,3,4,*]

[1]Howard Hughes Medical Institute, Department of Biomedical Engineering and Center of Synthetic Biology, Boston University, Boston, MA 02215, USA

[2]Program in Molecular Biology, Cell Biology, and Biochemistry, Boston University, Boston, MA 02215, USA

[3]Boston University School of Medicine, 715 Albany Street, Boston, MA 02118, USA

[4]Wyss Institute for Biologically Inspired Engineering, Harvard University, Boston, MA 02118, USA

Abstract

A declining pipeline of clinically useful antibiotics has made it imperative to develop more effective antimicrobial therapies, particularly against difficult-to-treat Gram-negative pathogens. Silver has been used as an antimicrobial since antiquity, yet its mechanism of action remains unclear. Here, we show that silver disrupts multiple bacterial cellular processes, including disulfide bond formation, metabolism and iron homeostasis. These changes lead to increased production of reactive oxygen species (ROS) and increased membrane permeability of Gram-negative bacteria, that can potentiate the activity of a broad range of antibiotics against Gram-negative bacteria in different metabolic states, as well as restore antibiotic susceptibility to a resistant bacterial strain. We show both *in vitro* and in a mouse model of urinary tract infection that the ability of silver to induce oxidative stress can be harnessed to potentiate antibiotic activity. Additionally, we demonstrate *in vitro* and in two different mouse models of peritonitis that silver sensitizes Gram-negative bacteria to the Gram-positive specific antibiotic, vancomycin, thereby expanding the antibacterial spectrum of this drug. Finally, we used silver and antibiotic combinations *in vitro* to eradicate bacterial persister cells, and show both *in vitro* and in a mouse biofilm infection model, that silver can enhance antibacterial action against biofilms. This work shows that silver can be used to enhance the action of existing antibiotics against Gram-negative bacteria thus strengthening the antibiotic arsenal for fighting bacterial infections.

INTRODUCTION

There is a growing need to enhance our antibacterial arsenal given the rising incidence of antibiotic resistance and the emergence of new virulent pathogens (1, 2). This is particularly true for infections caused by Gram-negative bacteria, which are difficult to treat because these organisms possess a protective outer membrane consisting of lipopolysaccharides (3). Drug-resistant, Gram-negative bacterial infections have forced clinicians to revisit the use of

*Corresponding author: James J. Collins; jcollins@bu.edu; phone: (617) 353-0390..

AUTHOR CONTRIBUTIONS All authors designed the study, analyzed results, and wrote the manuscript. J.R.M.R performed experiments to identify the MOA of silver and assess its toxicity, designed and performed animal infection model experiments and synergy studies in both metabolic states. J.A.W. aided in the design of the *in vitro* experiments to determine synergy between antibiotics and resensitization of resistant strains. C.S.S. aided in the design and execution of all animal infection model experiments.

COMPETING INTERESTS The authors have no competing interests.

older antimicrobials that have previously been discarded (4–6). Silver is intriguing as its antimicrobial properties were first documented around 400 B.C. when Hippocrates described its use to enhance wound healing and preserve water and food (7). Despite this long-standing history and its demonstrated activity against Gram-negative bacteria, the complete bactericidal mode of action of silver remains unclear (8–16). Here we use a systems-based approach to identify the mechanistic effects of silver on Gram-negative bacteria. We then harness these mechanisms to potentiate and expand the activity of existing antibiotics.

RESULTS

Ag^+ induces OH• production and increases membrane permeability

We used ionic silver (Ag^+) in a silver nitrate salt ($AgNO_3$), and found substantial antimicrobial activity (~3 log) at 30 μM against log-phase growing *Escherichia coli,* a model Gram-negative bacterium (Fig. 1A and table S1). Production of reactive oxygen species (ROS), such as hydroxyl radicals (OH•), may be a common mechanism of cell death induced by bactericidal antibiotics (17–22), although the role of ROS in antibiotic-induced bacterial killing is a matter of debate (23, 24). We measured hydroxyl radicals in untreated *E. coli* cells and in cells treated with Ag^+ for one hour, using 3'-(p-hydroxyphenyl) fluorescein (HPF) dye (25). Ag^+-treated cells exhibited detectable increases in fluorescence compared to untreated cells, indicating increased OH• production (Fig. 1B). Moreover, reducing ROS through the addition of thiourea, an ROS scavenger (26) (fig. S1A), or by overexpressing superoxide dismutase (*sodA*) (fig. S1B), inhibited Ag^+-induced bacterial cell death, confirming that ROS production may be critical for the observed bactericidal activity.

Hydroxyl radicals are a product of Fenton chemistry, where free iron plays a key role (27). We measured the effect of Ag^+ on iron homeostasis by using an engineered promoter *E. coli* strain that produces the green fluorescent protein (GFP) in response to Fur, a master regulator of iron metabolism (22). After one hour of Ag^+ treatment, the reporter strain exhibited increased fluorescence relative to untreated cells (fig. S2A), indicating a disruption in iron concentrations within the cell. We then studied the effect of Ag^+ on two mutant *E. coli* strains with impaired iron regulation: a Δ*tonB* strain which has a blocked exogenous iron uptake system (28) and a Δ*iscS* strain which exhibits a smaller number of internal Fe-S clusters (29). Δ*tonB* had similar sensitivity to Ag^+ as the wildtype strain, whereas Δ*iscS* exhibited a bacteriostatic phenotype when subjected to Ag^+ treatment (Fig. 1C). Δ*iscS* also exhibited significantly lower OH• production ($p<0.001$) in response to Ag^+ treatment compared to the treated wildtype cells (fig. S2B). These results suggest that internal iron from Fe-S clusters plays a role in Ag^+-mediated cell death.

Transition metals, such as silver, copper and zinc, can break down or inactivate Fe-S clusters (30, 31) and cause leakage of Fe^{+2}. We therefore tested the ability of silver to disrupt Fe-S clusters and cause release of Fe^{+2} by measuring Fe^{+2} concentrations using Ferene-S, a colorimetric dye (32), in an Ag^+-treated *E. coli* cell lysate. We compared the absorbance to a positive control, a cell lysate heated to 90 °C to disrupt Fe-S clusters, and a negative control, an untreated lysate. Ag^+-treated lysates showed significantly higher Fe^{+2} concentrations relative to the untreated lysate ($p<0.001$) (Fig. 1D), demonstrating that Ag^+ directly interacts with and disrupts Fe-S clusters. Since stress-induced superoxide is also known to disrupt Fe-S clusters (22), we measured the response of a *soxS* reporter strain, which expresses GFP upon activation of SoxR by superoxide, to Ag^+ treatment and found that Ag^+ does indeed induce superoxide production (fig. S3). This result suggests that Ag^+ also indirectly leads to Fe^{+2} leakage by stimulating the production of superoxide. Together these findings indicate that Ag^+ disturbs internal iron homeostasis by directly and indirectly disrupting intracellular Fe-S clusters.

Superoxide is formed as a by-product of electron transfer through the electron transport chain (ETC) (33). The ETC component cytochrome *bd*-I oxidase has been shown to be crucial for superoxide production under conditions of stress (34). We therefore explored whether cytochrome *bd* is one of the sources of Ag^+-mediated superoxide production. We found that a cytochrome *bd* knockout strain (Δ*cydB*) was 10 times less sensitive to a 1h Ag^+ treatment than wildtype (Fig. 1E) and exhibited ~3 times lower concentrations of superoxide in response to the treatment (Fig. 1F), indicating that cytochrome *bd* is a source of Ag^+-mediated superoxide production.

We also explored the role of the TCA cycle, a metabolic pathway that feeds the ETC, in Ag^+-induced cell death. We examined cell viability and OH• production in Ag^+-treated TCA cycle gene knockout strains (Δ*icdA,* Δ*sucB,* Δ*mdh,* Δ*acnB*), and observed that all the knockout strains were less sensitive to Ag^+ treatment than wildtype (Fig. 1G). Additionally, there was a distinct correlation between the Ag^+-induced percent change in OH• production in the mutant strains and their susceptibility to Ag^+ (Fig. 1H), indicating that a functional TCA cycle facilitates Ag^+-mediated OH• production. These findings show that Ag^+ disrupts metabolic pathways that drive Fenton chemistry and lead to the overproduction of OH• and cell death.

We next used transmission electron microscopy (TEM) to explore the physical changes that occur to bacterial cells as a result of Ag^+ treatment (Fig. 2A and fig. S4A–C). Ag^+ treatment at bactericidal concentrations caused protein aggregation, indicated by the high density aggregates observed within the *E. coli* (10) and drastic morphological changes in the cell envelope. We reasoned that the observed Ag^+-induced physical alterations in cell morphology could be indicative of an overall increase in outer membrane permeability. To explore this, we used propidium iodide (PI), a membrane-impermeable fluorescent dye that has been utilized to detect permeation of the cell membrane (see Supplemental Methods and fig. S5). Ag^+-treated cells showed increased PI fluorescence relative to untreated cells, indicating destabilization of the cellular envelope and increased membrane permeability (Fig. 2B).

The protein aggregates observed in the TEM images of Ag^+-treated cells suggest the occurrence of protein misfolding. Ag^+ is capable of strongly interacting *in vitro* with sulphydryl (-SH) groups found in a variety of proteins (35). These functional groups form disulfide bonds in many proteins, which contribute to their overall shape, functionality and stability. We hypothesized that Ag^+ disrupts disulfide bond formation *in vivo*, which would contribute to protein misfolding and aggregation. To monitor disulfide bond formation during Ag^+ treatment, we used a *dps* reporter strain (fig. S6) that expresses GFP when the protein OxyR forms a disulfide bond in the presence of H_2O_2 (36). We treated the reporter strain with H_2O_2, Ag^+, and a combination of both (Fig. 2C). As expected, cells treated with H_2O_2 showed significantly increased fluorescence relative to untreated cells. The addition of Ag^+ to the H_2O_2 treatments reduced the fluorescence back to untreated levels, indicating that Ag^+ is capable of inhibiting or disrupting protein disulfide bond formation *in vivo*.

We next explored whether disrupting protein disulfide bond formation can affect membrane permeability. Disulfide bond formation is mediated by DsbA, a disulfide oxidoreductase. We found that an untreated Δ*dsbA* strain was more permeable than an untreated wildtype strain (fig. S7), indicating that impairment of disulfide bond formation is sufficient for increasing permeability. Furthermore, we tested the effect of Ag^+ on the Δ*dsbA* strain, since it exhibits a higher frequency of proteins with exposed sulphydryl groups (37), and found that it was more sensitive (Fig. 2D) and more permeable (Fig. 2E) than the Ag^+-treated wildtype strain. Knocking out DsbC, the enzyme responsible for disulfide bond repair, resulted in a phenotype similar to that exhibited by Δ*dsbA* (Fig. 2D).

Ag^+-induced misfolded proteins that are secreted from the cytoplasm and transported to the outer membrane could lead to the observed membrane destabilization and increased permeability (38). We evaluated the effect of Ag^+ on a Δ*secG* strain, which exhibits an impaired protein translocation machinery (39), and found that it was less permeable (Fig. 2E) and less susceptible to Ag^+ treatment (Fig. 2F) compared to wildtype. These results indicate that the translocation of misfolded proteins contributes to Ag^+-mediated cellular membrane permeability. These findings indicate that Ag^+ targets and disrupts multiple cellular processes, including disulfide bond formation, central metabolism and iron homeostasis and that these changes are associated with increases in ROS production and bacterial membrane permeability.

Ag^+ potentiates bactericidal antibiotics both *in vitro* and *in vivo*

We next explored the possibility of using Ag^+ as an antibiotic adjuvant, harnessing different mechanistic features of its mode of action. We first reasoned that the capacity of Ag^+ to disrupt metabolic processes and iron homeostasis would enable it to potentiate bactericidal antibiotics that share a common mechanism of action involving the overproduction of ROS (18). We treated *E. coli* with low, sublethal concentrations of gentamicin (an aminoglycoside antibiotic), ampicillin (a beta-lactam antibiotic), and ofloxacin (a quinolone antibiotic) (table S1). When we added sublethal concentrations of Ag^+ to these antibiotic treatments, we observed significantly enhanced antimicrobial activity ($p<0.001$) (Fig. 3A, fig. S8A–C and table S3). We used the Bliss Model to determine the nature of the therapeutic effects exhibited by the drug combinations (40, 41). We quantified the degree of synergy at 1 and 3 h between Ag^+ and each of the individual antibiotics and found their interactions to be synergistic for all cases (fig. S9). We also measured OH• in the treated cells and observed no detectable increases in ROS production resulting from the sublethal antibiotic treatments (Fig. 3B). However, the addition of sublethal doses of Ag^+ to the antibiotic treatments induced dramatic increases in ROS, suggesting that Ag^+ can prime cells for ROS production ($p<0.001$) (Fig. 3B). Together, these results indicate that the ability of Ag^+ to stimulate Fenton chemistry can be harnessed to potentiate the activity of antibiotics that utilize ROS as part of their bactericidal mechanism.

We also examined whether the ability of Ag^+ to increase membrane permeability could be exploited to enhance the intracellular influx of antibiotics. We first tested if Ag^+-mediated cell membrane permeability could be used to restore drug sensitivity to bacterial strains that have developed resistance through activation of efflux pumps and decreased antibiotic permeation. To test this possibility, we used an *E. coli* strain (AG112) that contains a mutation in the *marR* gene, which renders the strain resistant to multiple antibiotics, including the bacteriostatic drug tetracycline (42). We found that AG112 exhibits a 3-fold higher tetracycline minimum inhibitory concentration (MIC) than the wildtype (AG110) *E. coli* strain (Fig. 3E and table S4). Importantly, treating AG112 with a sub-inhibitory concentration of Ag^+ (15 μM) in combination with tetracycline restored the resistant strain's tetracycline MIC to wildtype levels (Fig. 3E). These data show that Ag^+ can enhance the antibiotic susceptibility of drug-resistant cells, potentially by increasing membrane permeability to the antibiotic.

As noted earlier, infections caused by Gram-negative bacteria are often difficult to treat (2). These bacteria have a protective outer membrane that prevents the entry of a variety of larger antibiotics, such as the glycopeptide vancomycin (3). We reasoned that the ability of Ag^+ to increase outer membrane permeability could be used to render vancomycin active against Gram-negative bacteria, thereby broadening the antibacterial spectrum and clinical utility of this antibiotic. We treated *E. coli* with low doses of Ag^+ and vancomycin individually and in combination, and found that the combination treatments resulted in significantly greater ($p<0.001$) bacterial cell death relative to treatments with Ag^+ or

vancomycin alone (Fig. 3C, fig. S10A–C and table S5). Using the Bliss Model, we determined the antimicrobial effects between Ag^+ and vancomycin to be synergistic at all of the concentrations tested (fig. S11). Moreover, the increased cell death we observed correlated with increases in membrane permeability resulting from the addition of Ag^+ (Fig. 3D). These results indicate that Ag^+ can be combined with vancomycin to form a drug combination that harnesses Ag^+-induced outer membrane permeability changes to enable vancomycin to become effective against Gram-negative bacteria.

We next examined whether the doses of Ag^+ used in this study have a toxic effect on mammalian systems. We first assessed Ag^+ toxicity *in vitro,* using an MTT cell viability assay on different human primary cells and cell lines. Our results showed that the cells exhibited no change in viability upon direct exposure to the Ag^+ concentrations used in this work (Fig. 4A). While Ag^+ is currently approved by the FDA as a topical antimicrobial (43), we investigated the possibility of using Ag^+ as an adjuvant in combination therapies through other delivery routes (i.e., intraperitoneally). Ag^+ toxicity delivered intraperitoneally was measured *in vivo* by determining the median lethal dose (LD_{50}), which is the drug dose at which 50% of the treated mice survive (Fig. 4B). We determined an LD_{50} between 120 and 240 μM, a result that is consistent with those of earlier toxicity studies (44). A standard way to establish the safety and efficiency of a drug is through the therapeutic index (ratio between LD_{50} and therapeutic concentrations) (45, 46). Based on our results, we calculated a therapeutic index for Ag^+ that ranges between 8 and 16, an index that is well within the ranges of the therapeutic indices reported for FDA-approved antibiotics, such as vancomycin (45), tobramycin, gentamicin, colistin and polymixin B (46).

We next evaluated the effects of Ag^+ on the blood chemistry and organ function of healthy, infection-free mice 6, 24 and 48 hours after treatment, by measuring key metabolite and enzyme concentrations using the Piccolo® Comprehensive Metabolic Reagent Disk from Abaxis (fig. S12A, B). Mice treated with Ag^+ showed normal kidney and pancreatic function, as well as normal concentrations of ions and trace metals (fig. S13A–D). We observed increased concentrations of the hepatic enzymes alkaline phosphatase (ALP) and alanine aminotransferase (ALT) (fig. S13B) at the initiation of treatment; however, the mice stabilized and recovered to concentrations within the normal range 48 hours after treatment (fig. S14A, B). Elevated hepatic enzyme concentrations have been considered safe if they are reversible and not accompanied by increases in total bilirubin (47). Total bilirubin concentrations remained within normal limits throughout the Ag^+ treatments (fig. S13B). While further studies are needed to fully determine the toxicity of Ag^+, these *in vivo* results suggest that the Ag^+ dosages used in this study are well tolerated by mice.

We utilized a mouse model of acute peritonitis to examine whether the mechanistic effects of Ag^+ observed *in vitro* (increased membrane permeability and OH• production) are also observed *in vivo* following Ag^+ treatment (Fig. 5A). One hour following inoculation of the bacteria into the peritoneal cavity, the mice were treated with either PBS or 30 μM Ag^+ delivered intraperitoneally. One hour post-treatment, the bacteria within the peritoneal cavity were collected and tested for OH• production and increased permeability using HPF and PI dyes, respectively (Fig. 5B). Treating mice with Ag^+ increased both HPF (Fig. 5C) and PI (Fig. 5D) fluorescence of the bacteria in the intraperitoneal cavity, demonstrating that Ag^+ treatment increases hydroxyl radical production and bacterial cell wall permeability *in vivo* (Fig. 5). Based on these results, we hypothesized that low doses of Ag^+ may be able to potentiate antibiotic activity *in vivo*.

We first examined whether Ag^+ could potentiate gentamicin activity *in vivo* by testing the effects of Ag^+ and gentamicin individually and in combination on a mouse urinary tract infection (UTI) model. UTI infections are one of the most commonly occurring infections in

clinical settings (48). The infection was established in the bladder through transurethral catheterization and delivery of 2×10^9 MG1655 *E. coli* cells suspended in an aqueous solution containing mucin (Fig. 6A). 24 hours post-infection, the mice received no treatment or intraperitoneally-administered gentamicin, Ag^+, or gentamicin plus Ag^+. Treatment with gentamicin or Ag^+ alone resulted in no effect on bladder *E. coli* cell counts 24 hours post-treatment related to the control, whereas treatment with gentamicin plus Ag^+ reduced the cell counts by 4-fold (Fig. 6B–C). These results demonstrate that Ag^+ is capable of potentiating antibiotic activity *in vivo*.

We also examined whether Ag^+ could potentiate vancomycin activity *in vivo*. We analyzed the effects of Ag^+ and vancomycin individually and in combination in both an acute and mild mouse model of peritonitis. The infection was established in the peritoneal cavity through intraperitoneal injection of either 1×10^4 MG1655 *E. coli* cells (mild model) (Fig. 7A) or 5×10^6 MG1655 *E. coli* cells (acute model) (Fig. 7C), suspended in an aqueous solution containing mucin. One hour (for acute infection model) and 24 hours (for mild infection model) post-infection, the mice received either no treatment or intraperitoneal delivery of vancomycin, Ag^+, or vancomycin plus Ag^+. We monitored two aspects of the infection: the *E. coli* cell counts within the peritoneal cavity (in both models) and mouse survival (only for the acute peritonitis model since the mild infection model was not lethal). In the mild peritonitis model, the combination of Ag^+ plus vancomycin led to a significant cell count reduction relative to the control (Fig. 7B). In the acute model, we observed that treatment with vancomycin or Ag^+ alone resulted in no effect on intraperitoneal *E. coli* cell counts after 24 hours, whereas treatment with vancomycin plus Ag^+ reduced the cell counts by 100-fold (Fig. 7D). Additionally, in the acute intraperitoneal model, 90% of mice treated with the vancomycin-plus-Ag^+ combination survived (after 5 days), compared with 50% of mice treated with Ag^+ alone and 10% of mice treated with vancomycin alone or just the vehicle (Fig. 7E). These findings demonstrate the possibility of using Ag^+ to enhance the activity of vancomycin against Gram-negative pathogens *in vivo*.

Ag^+ potentiates bactericidal antibiotics against bacterial persisters and biofilms

Bacterial persisters, which are dormant cells within an isogenic bacterial population that are tolerant to antibiotic treatment, are thought to play an important role in chronic recurring infections and the formation of biofilms. Both of these represent an important economic burden for the health care industry, since they directly contribute to increased hospital visits from patients with deteriorating health conditions. This has stimulated research to find viable ways to treat and eliminate bacteria persisters (49, 50). We explored the effect of Ag^+ on bacterial persisters *in vitro*. We treated *E. coli* persister cells with a range of Ag^+ concentrations and found increased antimicrobial activity above 60 μM (Fig. 8A). We next measured HPF and PI fluorescence in untreated persister cells and cells treated for 3 h with lethal (60 μM) and sub-lethal (30μM) Ag^+ concentrations. Ag^+-treated cells showed increases in both HPF (Fig. 8B) and PI (Fig. 8C) fluorescence compared to untreated bacterial persisters. These results, in combination with data noted above, provide evidence that Ag^+ treatment drives increased production of ROS and increased permeability of bacteria in both active and dormant metabolic states.

Based on the effects and mechanisms observed in bacterial persister cells after treatment with Ag^+, we hypothesized that Ag^+ also may be able to potentiate antibiotic activity against bacterial persister cells. We treated *E. coli* persister cells with sublethal concentrations of Ag^+(30μM) and three different antibiotics (ampicillin at 10μg/mL, ofloxacin at 3μg/mL, and gentamicin at 5μg/mL) individually and in combination, and observed that the combination treatments exhibited greater bactericidal activity relative to the individual treatments with Ag^+ or each of the antibiotics (Fig. 8D–F). Using the Bliss Model, we determined that the antimicrobial effects were synergistic between Ag^+ and the individual antibiotics tested (fig.

S15). Together these results indicate that the multifaceted bactericidal mode of action of silver can be harnessed to enable antibiotics to kill bacterial persister cells.

Biofilms, implicated in chronic infections of the urinary tract, lungs, skin, and other areas of the body, represent a clinical challenge due to difficulties in treating them (51). We explored the possibility of using the Ag^+-gentamicin combinatorial therapy to treat biofilms grown *in vitro*. *E. coli* biofilms grown overnight were treated with Ag^+ and gentamicin individually and in combination. We observed that the combination treatment resulted in greater bacterial cell death relative to the treatments with Ag^+ or gentamicin alone (Fig. 9A–D).

Next we utilized a mouse biofilm infection model to determine whether the potentiated bactericidal effects exhibited *in vitro* would be observed in an *in vivo* setting. Biofilms were grown in catheters that were surgically implanted subcutaneously in mice. 48 h after the catheters were implanted, the mice received no treatment or intraperitoneally-delivered gentamicin, Ag^+, or gentamicin plus Ag^+ (Fig. 9E). The catheters were surgically removed from the mice 24 h after treatment and the bacterial counts showed that treatment with gentamicin presented no difference compared to the untreated control, whereas treatment with Ag^+ alone showed a slight decrease of less than 10-fold when compared to the untreated control (Fig. 9F). Interestingly, the combination therapy (gentamicin plus Ag^+) reduced cell counts in the biofilms by more than 100-fold compared to the untreated control ($p<0.001$) (Fig. 9F). These results demonstrate the capability of Ag^+ to potentiate antibiotic activity against biofilms in *in vivo* settings.

DISCUSSION

By conducting phenotypic and genetic analyses, both *in vitro* and *in vivo*, we show that Ag^+, an ancient antibacterial agent, disrupts multiple bacterial cellular networks and processes, resulting in the destabilization of the cellular envelope and the production of ROS in Gram-negative bacteria. Our work suggests that this multi-targeted antimicrobial mechanism of action is the result of silver's thiophilic chemical properties. Through exploitation of these mechanistic effects, we demonstrate that Ag^+ can potentiate the activity of a broad range of antibiotics against Gram-negative bacteria in distinct metabolic states, establishing it as a potent antibiotic adjuvant.

Multidrug-resistant, Gram-negative bacteria are an important cause of nosocomial infections. Our data show that Ag^+ has an antimicrobial synergistic effect against Gram-negative bacteria when used in combination with beta-lactams, aminoglycosides, and quinolones. Furthermore, our work indicates that combination therapies involving Ag^+ and large antibiotics such as vancomycin may be an option for treating Gram-negative infections. More generally, the ability of Ag^+ to permeabilize the outer membranes of Gram-negative bacteria may enable repurposing of existing drugs to enhance the current antibiotic arsenal.

In this work, we studied the effects of silver at inhibitory and lethal concentrations. We show using transmission electron microscopy, that even at sublethal Ag^+ concentrations we can observe moderate morphological changes in the membrane and protein aggregates. Additionally, we demonstrate that the main phenotypes – increases in ROS production and membrane permeability – are triggered at both inhibitory and lethal silver concentrations. Further we show that the moderate increases in membrane permeability and ROS production caused by sublethal concentrations of silver can be used to enhance the activity of antibiotics and broaden the spectrum of vancomycin. We hypothesize that the increases in ROS production are likely an indirect effect of the interaction of silver with its targets; this is supported by our findings that mutant strains that impair the primary effects of silver exhibit

diminished antibiotic susceptibility and decreased ROS production. As noted earlier, two recent papers questioned the role of the ROS in antibiotic-mediated bacterial cell death (23, 24), though methodological concerns about these studies have been raised (52, 53). Here we show, using multiple assays and experiments, that silver treatment leads to ROS production in bacteria and that this effect can be harnessed to enhance the killing efficacy of bactericidal antibiotics *in vitro* and *in vivo*.

Even though Ag^+ interacts with the microbial cell at multiple sites, resistance has been observed in some cases (54, 55) mainly through overexpression of copper-related efflux pumps. However, because antibacterial combination therapies involving low doses of Ag^+ would induce cell death through the attack of multiple cellular sites, such approaches could potentially delay the emergence of resistance (56–58).

The synergistic effect between Ag^+ and the different antibiotics is achieved when adding 15 and 30 μM Ag^+, for metabolically active and non-active cells, respectively. These Ag^+ concentrations correspond to a two-fold decrease when compared to the active concentration of Ag^+ required to treat in the absence of antibiotics. This suggests that those concentrations of Ag^+ are necessary to trigger enough membrane permeability and/or ROS production to synergize with the antibiotics. Of note, silver has been used successfully in topical therapeutic ointments. Moreover, our results describing the capability of silver to enhance antibiotic activity across a wide range of antibiotics, in combination with the toxicity data, invites a future study of its use as an antibiotic adjuvant that can be orally taken or injected and used in a wider clinical setting. We are optimistic that future work from the fields of drug delivery and bionanotechnology will use new compounds containing Ag^+ to develop more efficient and sophisticated therapies. Such could be the case for silver in its nanoparticle form (8), which has been shown to be a more effective antimicrobial agent when compared to Ag^+. Moreover, given recent advances in nanotechnology and surface chemistry, we can envision synthesizing silver nanoparticles with antibiotic-decorated surfaces within an intelligent material that controls release of active antimicrobial compounds at the site of infection.

MATERIALS AND METHODS

For all experiments performed with cells in exponential phase, *E. coli* overnight cultures were diluted 1:250 in 25mL of Luria-Bertani (LB) media and grown to an OD_{600nm} of 0.3 in 250 mL flasks at 37 °C, 300 rpm, and 80% humidity. All antimicrobial treatments were performed in 500 μL samples in 24-well plates incubated at 37 °C, 900 rpms, and 80% humidity. For experiments with bacterial persister cells, *E. coli* were grown to stationary phase for 16 h at 37 °C, 300 rpm, and 80% humidity in 25 mL of LB. Cells were then treated with 5 μg/mL ofloxacin for 4 h to kill non-persister cells. The samples were then washed with PBS and suspended in M9 minimal media and treated with the different antibiotics to determine killing of persisters. For experiments with biofilms, an *E. coli* culture grown overnight was diluted 1:200 into MBEC Physiology and Genetic Assay wells (MBEC BioProducts, Edmonton, Canada) and grown for 24 h at 30 °C, 0 rpm and 80% humidity. All wells containing biofilms were then treated with the different antibiotics. After treatment, the wells were washed with PBS 3x and then sonicated for 45 min in order to disrupt the biofilm and plate cells to count colony-forming units (cfu). Unless otherwise specified, the following concentrations were used in the *E. coli* antimicrobial treatments: 10, 20, 30, 60 and 120 μM silver nitrate, 0.25 μg/mL and 5 μg/mL gentamicin, 1 μg/mL and 10μg/mL ampicillin, 0.03 μg/mL and 3 μg/mL ofloxacin, and 30 μg/mL vancomycin. Kill curves for the antimicrobial treatments were obtained by spot-plating serially diluted samples and counting cfu. Gene knockout strains were constructed by P1-phage transduction from the Keio knockout mutant collection. Raw data (cfu/mL) for killing assays for all

strains are in table S2. Construction of the genetic reporter strains for iron misregulation, superoxide production and disulfide bond formation, as well as the *sodA* overexpression strain, was performed using conventional molecular cloning techniques. The fluorescent reporter dye 3'-(p-hydroxyphenyl fluorescein (HPF) was used as previously described (18) at 5 mM to detect hydroxyl radical (OH•) formation. The fluorescent dye, propidium iodide (PI), was used at concentrations of 1 mM to monitor membrane permeability. Fluorescence data were collected using a Becton Dickinson FACSCalibur flow cytometer. For the permeability and OH• production assays, fluorescence of the respective dyes was determined as a percent change using the following formula: $((\text{Fluorescence}_{\text{dye}} - \text{Fluorescence}_{\text{no dye}})/(\text{Fluorescence}_{\text{no dye}}))*(100)$. For the OH• quenching experiments, cells were treated with 150mM thiourea and $AgNO_3$ simultaneously. Release of protein-bound iron in an *E. coli* cell lysate was detected by incubating samples for 1 h in a 10 mM Ferene-S assay and measuring absorbance at 593 nm. The lysates were prepared by sonication in 20 mM Tris/HCl pH 7.2 buffer. The lysates were treated either with heat (90 °C for 20 min) or $AgNO_3$ (30 μM for 1 h). All samples analyzed with the Jeol 1200EX – 80kV transmission electron microscope were fixed utilizing glutaraldehyde, dehydrated using ethanol, embedded using spur resin, and microtomed in ~60 nm thickness samples. Mouse experiments were performed with male Charles River mice as described in the main text and the *in vivo* studies section below.

Supplementary Material

Refer to Web version on PubMed Central for supplementary material.

Acknowledgments

We thank the members of the Collins Lab for helpful discussions and Cristobal Guerra for his help with some of the figure illustrations. We also thank Maria Ericsson at the Harvard Medical School Cell Biology Electron Microscopy Facility, the ARCH animal facilities at Harvard Children's Hospital, and the Wyss Institute for their animal and research facilities.

FUNDING Supported by the NIH Director's Pioneer Award Program and the Howard Hughes Medical Institute.

REFERENCES

1. Taubes G. The bacteria fight back. Science. 2008; 321:356. [PubMed: 18635788]
2. Li J, et al. Colistin: the re-emerging antibiotic for multidrug-resistant Gram-negative bacterial infections. Lancet Infect. Dis. 2006; 6:589. [PubMed: 16931410]
3. Pages JM, James CE, Winterhalter M. The porin and the permeating antibiotic: a selective diffusion barrier in Gram-negative bacteria. Nature Reviews Microbiology. 2008; 6:893.
4. Li J, et al. Colistin: the re-emerging antibiotic for multidrug-resistant Gram-negative bacterial infections. Lancet Infectious Diseases. 2006; 6:589. [PubMed: 16931410]
5. Falagas ME, Kasiakou SK. Colistin: the revival of polymixins for the management of multidrug-resistant Gram-negative bacterial infections. Clinical Infectious Diseases. 2005; 40:1333. [PubMed: 15825037]
6. Kasiakou SK, et al. Combination therapy with intravenous colistin for management of infections due to multidrug-resistant Gram-negative bacteria in patients with cystic fibrosis. Antimicrobial Agents and Chemotherapy. 2005; 49:3136. [PubMed: 16048915]
7. Magner, LN. Hippocrates and the Hippocratic Tradition. A History of Medicine. Duffy, J., editor. Marcel Dekker, Inc; NYC: 1992. p. 393
8. Morones JR, et al. The bactericidal effect of silver nanoparticles. Nanotechnology. 2005; 16:2346. [PubMed: 20818017]
9. Thurman RB, Gerba CP. The molecular mechanisms of copper and silver ion disinfection of bacteria and viruses. CRC Critical Reviews in Environmental Control. 1988; 18:295.

10. Feng QL, et al. A mechanistic study of the antibacterial effect of silver ions on Escherichia coli and Staphylococcus aureus. J. Biomed. Mater. Res. 2000; 52:662. [PubMed: 11033548]
11. Jung WK, et al. Antibacterial activity and mechanism of action of the silver ion in Staphylococcus aureus and Escherichia coli. Appl. Environ. Microbiol. 2008; 74:2171. [PubMed: 18245232]
12. Slawson RM, Lee H, Trevors JT. Bacterial Interactions with Silver. Biology of Metals. 1990; 3:151. [PubMed: 2073456]
13. Holt KB, Bard AJ. Interaction of silver(I) ions with the respiratory chain of Escherichia coli: An electrochemical and scanning electrochemical microscopy study of the antimicrobial mechanism of micromolar Ag. Biochemistry. 2005; 44:13214. [PubMed: 16185089]
14. Park HJ, et al. Silver-ion-mediated reactive oxygen species generation affecting bactericidal activity. Water Research. 2009; 43:1027. [PubMed: 19073336]
15. Gordon O, et al. Silver coordination polymers for prevention of implant infection: Thiol interaction, impact on respiratory chain enzymes, and hydroxyl radical induction. Antimicrobial Agents and Chemotherapy. 2010; 54:4208. [PubMed: 20660682]
16. Randall CP, Oyama LB, Bostock JM, Chopra I, O'Neill AJ. The silver cation (Ag+): antistaphylococcal activity, mode of action and resistance studies. J. Antimicrob. Chemother. 2013; 68:131. [PubMed: 23011288]
17. Kohanski MA, Dwyer DJ, Collins JJ. How antibiotics kill bacteria: from targets to networks. Nature Reviews Microbiology. 2010; 8:423.
18. Kohanski MA, Dwyer DJ, Hayete B, Lawrence CA, Collins JJ. A common mechanism of cellular death induced by bactericidal antibiotics. Cell. 2007; 130:797. [PubMed: 17803904]
19. Dwyer DJ, Camacho DM, Kohanski MA, Callura JM, Collins JJ. Antibiotic-Induced Bacterial Cell Death Exhibits Physiological and Biochemical Hallmarks of Apoptosis. Mol. Cell. 2012; 46:561. [PubMed: 22633370]
20. Foti JJ, Devadoss B, Winkler JA, Collins JJ, Walker GC. Oxidation of the Guanine Nucleotide Pool Underlies Cell Death by Bactericidal Antibiotics. Science. 2012; 336:315. [PubMed: 22517853]
21. Kohanski MA, Dwyer DJ, Wierzbowski J, Cottarel G, Collins JJ. Mistranslation of Membrane Proteins and Two-Component System Activation Trigger Antibiotic-Mediated Cell Death. Cell. 2008; 135:679. [PubMed: 19013277]
22. Dwyer DJ, Kohanski MA, Hayete B, Collins JJ. Gyrase inhibitors induce an oxidative damage cellular death pathway in Escherichia coli. Molecular Systems Biology. 2007; 3
23. Liu Y, Imlay JA. Cell death from antibiotics without the involvement of reactive oxygen species. Science. 2013; 339:1210. [PubMed: 23471409]
24. Keren I, Wu Y, Inocencio J, Mulcahy LR, Lewis K. Killing by bactericidal antibiotics does not depend on reactive oxygen species. Science. 2013; 339:1213. [PubMed: 23471410]
25. Setsukinai K, Urano Y, Kakinuma K, Majima HJ, Nagano T. Development of novel fluorescence probes that can reliably detect reactive oxygen species and distinguish specific species. Journal of Biological Chemistry. 2003; 278:3170. [PubMed: 12419811]
26. Novogrodsky A, Ravid A, Rubin AL, Stenzel KH. Hydroxyl radical scavengers inhibit lymphocyte mitogenesis. Proceedings of the National Academy of Sciences of the United States of America-Biological Sciences. 1982; 79:1171.
27. Imlay JA, Chin SM, Linn S. Toxic DNA damage by hydrogen peroxide through the Fenton reaction *in vivo* and *in vitro*. Science. 1988; 240:640. [PubMed: 2834821]
28. Touati D, Jacques M, Tardat B, Bouchard L, Despied S. Lethal oxidative damage and mutagenesis are generated by iron in delta fur mutants of Escherichia coli: protective role of superoxide dismutase. Journal of Bacteriology. 1995; 177:2305. [PubMed: 7730258]
29. Schwartz CJ, Djaman O, Imlay JA, Kiley PJ. The cysteine desulfurase, IscS, has a major role in in vivo Fe-S cluster formation in Escherichia coli. Proceedings of the National Academy of Sciences of the United States of America. 2000; 97:9009. [PubMed: 10908675]
30. Xu FF, Imlay JA. Silver(I), mercury(II), cadmium(II), and zinc(II) target exposed enzymic iron-sulfur clusters when they toxify Escherichia coli. Appl. Environ. Microbiol. 2012; 78:3614. [PubMed: 22344668]

31. Chillappagari S, et al. Copper stress affects iron homeostasis by destabilizing iron-sulfur cluster formation in *Bacillus subtilis*. Journal of Bacteriology. 2010; 192:2512. [PubMed: 20233928]
32. Eskelinen S, Haikonen M, Raisanen S. Ferene-S as the chromagen for serum determinations. Scandinavian Journal of Clinical & Laboratory Investigation. 1983; 43:453. [PubMed: 6648330]
33. Korshunov S, Imlay JA. Two sources of endogenous hydrogen peroxide in Escherichia coli. Molecular Microbiology. 2010; 75:1389. [PubMed: 20149100]
34. Lindqvist A, Membrillo-Hernandez J, Poole RK, Cook GM. Roles of respiratory oxidases in protecting Escherichia coli K12 from oxidative stress. Antonie Van Leeuwenhoek International Journal of General and Molecular Microbiology. 2000; 78:23.
35. Liau SY, Read DC, Pugh WJ, Furr JR, Russell AD. Interaction of silver nitrate with readily identifiable groups: relationship to the antibacterial action of silver ions. Lett. Appl. Microbiol. 1997; 25:279. [PubMed: 9351278]
36. Zheng M, Aslund F, Storz G. Activation of the OxyR transcription factor by reversible disulfide bond formation. Science. 1998; 279:1718. [PubMed: 9497290]
37. Kadokura H, Katzen F, Beckwith J. Protein disulfide bond formation in prokaryotes. Annual Review of Biochemistry. 2003; 72:111.
38. Denoncin K, Vertommen D, Paek E, Collet JF. The protein-disulfide isomerase ΔsbC cooperates with SurA and ΔsbA in the assembly of the essential β-barrel protein LptD. Journal of Biological Chemistry. 2010; 285:29425. [PubMed: 20615876]
39. Matsumoto G, Mori H, Ito K. Roles of SecG in ATP- and SecA-dependent protein translocation. Proceedings of the National Academy of Sciences of the United States of America. 1998; 95:13567. [PubMed: 9811840]
40. Brynildsen MP, Winkler JA, Spina CS, MacDonald IC, Collins JJ. Potentiating antibacterial activity by predictably enhancing endogenous microbial ROS production. Nat Biotech. 2013; 31:160.
41. Hegreness M, Shoresh N, Damian D, Hartl D, Kishony R. Accelerated evolution of resistance in multidrug environments. Proc. Natl. Acad. Sci. U. S. A. 2008; 105:13977. [PubMed: 18779569]
42. Alekshun MN, Levy SB. Characterization of MarR superrepressor mutants. J. Bacteriol. 1999; 181:3303. [PubMed: 10322039]
43. FDA. www.accessdata.fda.gov/scripts/cder/drugsatfda
44. Dequidt J, Vasseur P, Gromez-Potentier J. Experimental toxicological study of some silver derivatives. Bulletin de la Societe de Pharmacie de Lille. 1974; 1:23.
45. Wold JS, Turnipseed SA. Toxicology of vancomycin in laboratory animals. Reviews of infectious diseases. 1981; 3(suppl):S224. [PubMed: 7342285]
46. Davis SD. Activity of gentamicin, tobramycin, polymyxin B, and colistimethate in mouse protection tests with Pseudomonas aeruginosa. Antimicrob Agents Chemother. 1975; 8:50. [PubMed: 169729]
47. Watkins PB, Seligman PJ, Pears JS, Avigan MI, Senior JR. Using Controlled Clinical Trials to Learn More About Acute Drug-Induced Liver Injury. Hepatology. 2008; 48:1680. [PubMed: 18853438]
48. Hung CS, Dodson KW, Hultgren SJ. A murine model of urinary tract infection. Nature protocols. 2009; 4:1230.
49. Allison KR, Brynildsen MP, Collins JJ. Metabolite-enabled eradication of bacterial persisters by aminoglycosides. Nature. 2011; 473:216. [PubMed: 21562562]
50. Vega NM, Allison KR, Khalil AS, Collins JJ. Signaling-mediated bacterial persister formation. Nature Chemical Biology. 2012; 8:431.
51. Lu TK, Collins JJ. Dispersing biofilms with engineered enzymatic bacteriophage. Proc. Natl. Acad. Sci. U. S. A. 2007; 104:11197. [PubMed: 17592147]
52. Hung D. How antibiotics kill bacteria: new models needed? Nat. Med. 2013; 19:544. [PubMed: 23652106]
53. Fang FC. Antibiotic and ROS linkage questioned. Nat Biotech. 2013; 31:415.
54. Garcia-Rivera J, Casadevall A. Melanization of Cryptococcus neoformans reduces its susceptibility to the antimicrobial effects of silver nitrate. Med. Mycol. 2001; 39:353. [PubMed: 11556765]

55. Gupta A, Matsui K, Lo JF, Silver S. Molecular basis for resistance to silver cations in Salmonella. Nat. Med. 1999; 5:183. [PubMed: 9930866]

56. Kitano H. A robustness-based approach to systems-oriented drug design. Nature Reviews Drug Discovery. 2007; 6:202.

57. Chait R, Craney A, Kishony R. Antibiotic interactions that select against resistance. Nature. 2007; 446:668. [PubMed: 17410176]

58. Cottarel G, Wierzbowski J. Combination drugs, an emerging option for antibacterial therapy. Trends in Biotechnology. 2007 25.

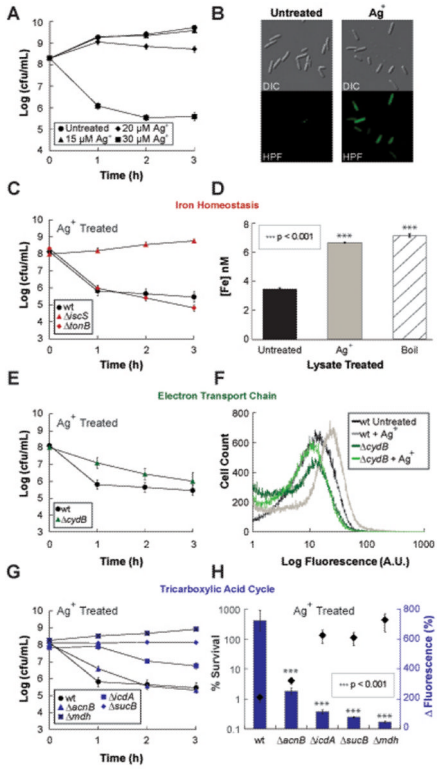

Fig. 1. Ag^{+} induces OH• production through a metabolic cascade and iron misregulation

(A) Kill curves for log-phase growing wildtype *E. coli* treated with various concentrations of $AgNO_3$. **(B)** Bright field and fluorescence microscopy of HPF-stained untreated *E. coli* cells and cells treated with 30 μM $AgNO_3$ after 1 h. **(C)** Survival of iron homeostasis gene knockout mutants relative to wildtype when treated with 30 μM $AgNO_3$. **(D)** Free iron [Fe^{+2}] concentration in a cell lysate after 1 h treatment with heat (90 °C) or 30 μM $AgNO_3$. **(E)** Survival of an electron transport gene knockout mutant relative to wildtype when treated with 30 μM $AgNO_3$. **(F)** GFP fluorescence histogram from the *soxS* reporter, incorporated into a wildtype and Δ*cydB* strain of *E. coli*, after 1 h treatment with 30 μM $AgNO_3$. **(G)** Survival of TCA cycle gene knockout mutants relative to wildtype when treated with 30 μM $AgNO_3$. **(H)** Blue bars show percent change in fluorescence for 3'-(p-hydroxyphenyl) fluorescein (hydroxyl radical production), HPF-stained wildtype and TCA cycle mutant strains of *E. coli* treated for 1 h with 30 μM $AgNO_3$ relative to the HPF-stained untreated strains. The diamond data points represent percent survival after 1 h of treatment with 30 μM $AgNO_3$. Error bars represent mean ± SEM for at least 3 biological replicates. *** indicates a p-value of <0.001 as determined by a student t-test, indicating a significant difference from the untreated lysate in (D) and the treated wildtype in (H).

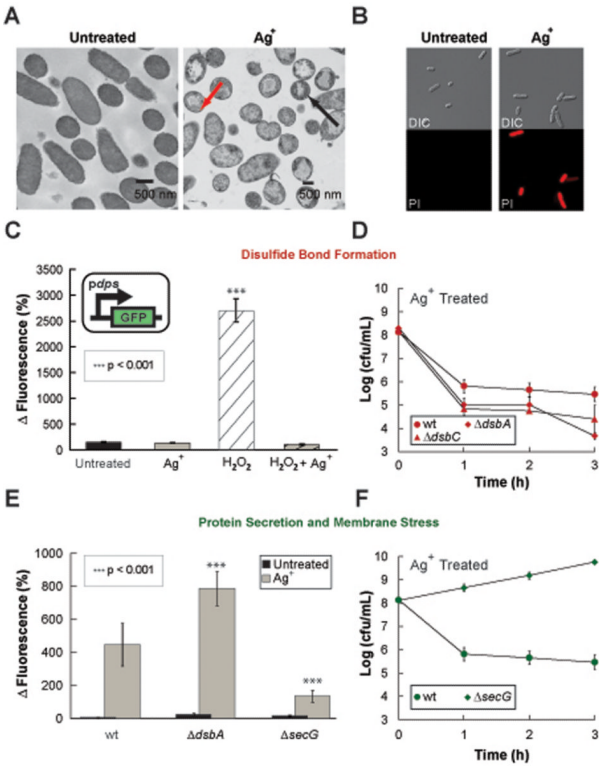

Fig. 2. Ag^+ increases membrane permeability through disruption of disulfide bond formation and misfolded protein secretion

(A) Transmission electron microscopy micrographs showing untreated (left) and 30 μM $AgNO_3$-treated *E. coli*. The red arrow indicates a cell showing outer membrane separation, which is indicative of membrane stress. The black arrow indicates a cell exhibiting protein aggregation (10). **(B)** Bright field and fluorescence microscopy of PI-stained untreated cells and cells treated for 1 h with 30 μM $AgNO_3$. **(C)** Change in green fluorescent protein (GFP) fluorescence from the disulfide bond genetic reporter strain after 1 h of the following treatments: 30 μM $AgNO_3$, 0.5 mM H_2O_2, and the combination of both. Values shown are relative to fluorescence at time zero before treatment. (*Inset*) Schematic of the reporter strain, which is based on activation of the *dps* promoter. **(D)** Survival of disulfide bond formation gene knockout mutants relative to wildtype when treated with 30 μM $AgNO_3$. **(E)** Change in fluorescence of propidium iodide (membrane permeability), PI-stained wildtype, Δ*dsbA*, and Δ*secG* strains of *E. coli* after 1 h treatment with 30 μM $AgNO_3$. **(F)** Survival of protein secretion gene knockout mutants relative to wildtype when treated with 30 μM $AgNO_3$. Error bars represent mean ± SEM for at least 3 biological replicates. *** indicates a p-value of <0.001 as determined by a student t-test, indicating a significant difference from the untreated control in (C) and the treated wildtype in (E).

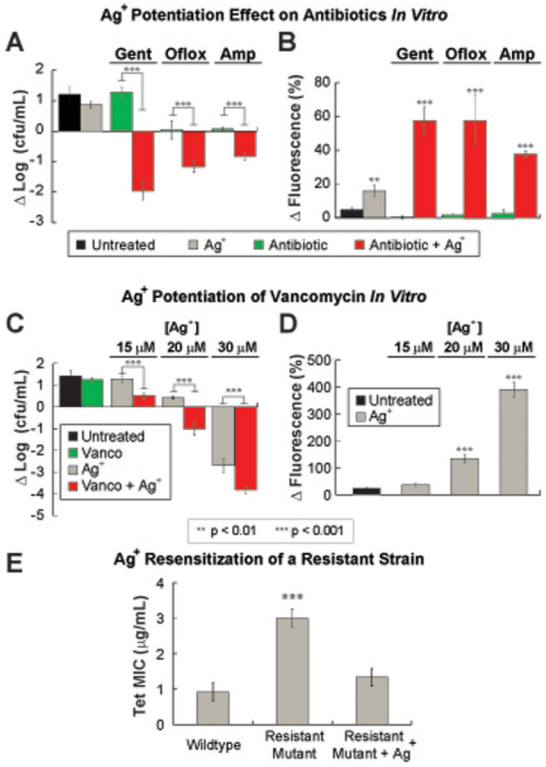

Fig. 3. Ag^+ potentiates bactericidal antibiotics *in vitro*

(A) Log change in cfu/mL, from time zero, of wildtype *E. coli* after treatment for 3 h with 15 μM $AgNO_3$, 0.25 μg/mL gentamicin, 0.03 μg/mL ofloxacin, 1 μg/mL ampicillin, and combinations of $AgNO_3$ with the respective antibiotics. **(B)** Changes in HPF fluorescence after 1 h of administering the treatments described in (A). **(C)** Log change in cfu/mL, from time zero, of wildtype *E. coli* after treatment for 3 h with the indicated concentrations of $AgNO_3$ and 30 μg/mL vancomycin. **(D)** Changes in PI fluorescence after 1 h of administering different concentrations of $AgNO_3$. Error bars represent mean ± SEM for at least 6 biological replicates. 10 mice per treatment group were used for the survival studies. **(E)** Treatment of a drug-resistant *E. coli* strain with Ag^+ restores antibiotic susceptibility back to wildtype levels. Tetracycline MIC of wildtype *E. coli* (AG100) and that of an *E. coli* drug-resistant strain (AG112) with and without Ag^+ treatment. *** indicates a p-value of <0.001 and ** indicates a p-value of <0.05 as determined by a student t-test, indicating a significant difference from the wildtype strain or untreated control, unless otherwise specified. Error bars represent mean ± SEM for at least 3 biological replicates.

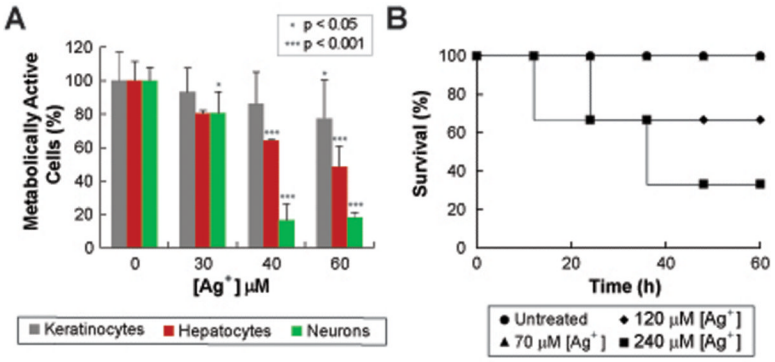

Fig. 4. Toxicity studies of Ag^+ showing that low levels of Ag^+ are not cytotoxic

(A) Percentage of metabolically active human cell lines (keratinocytes, hepatocytes and neurons) after being treated with increasing Ag^+ concentrations. **(B)** Survival of mice treated with: no treatment, 70 µM, 120 µM and 240 µM of $AgNO_3$. Survival studies were done using 10 mice per group. *** indicates a p-value of <0.001 and * indicates a p-value of <0.05 as determined by a student t-test, indicating a significant difference from the untreated control. Error bars represent mean ± SEM for at least 3 biological replicates.

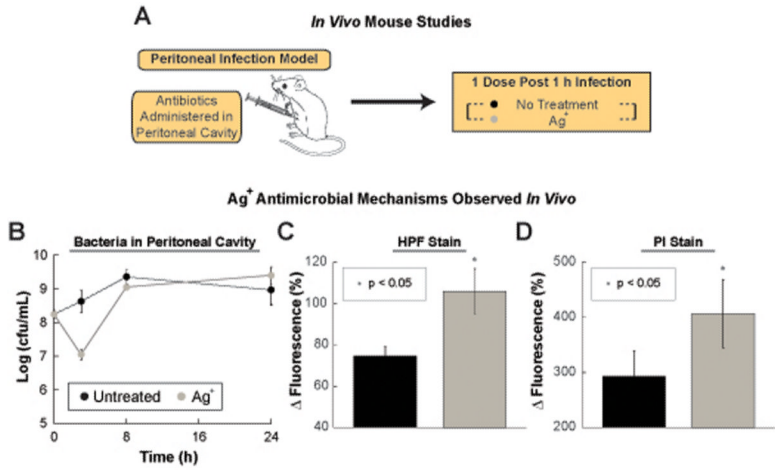

Fig. 5. Mode of action of Ag^+ in *in vivo* mild and acute peritonitis models

(A) Schematic of the *in vivo* animal experiments. **(B)** Bacterial counts in peritoneal cavity for experiment showing *in vivo* Ag^+ bactericidal mechanism of action. Kill curves of wildtype *E. coli* within the peritoneal cavity of mice after no treatment and treatment with 6 mg $AgNO_3$/kg body weight (35 μM). **(C)** Change in fluorescence of the HPF-stained and **(D)** PI-stained *E. coli* cells harvested from the peritoneal cavity of mice that have developed a peritoneal infection for 3 h and are treated 1 h after (4 h total after infection) with 6 mg $AgNO_3$/kg body weight (35 μM). Error bars represent mean ± SEM for at least 10 biological replicates. ** indicates a p-value of <0.05 as determined by a student t-test, indicating a significant difference from the untreated control.

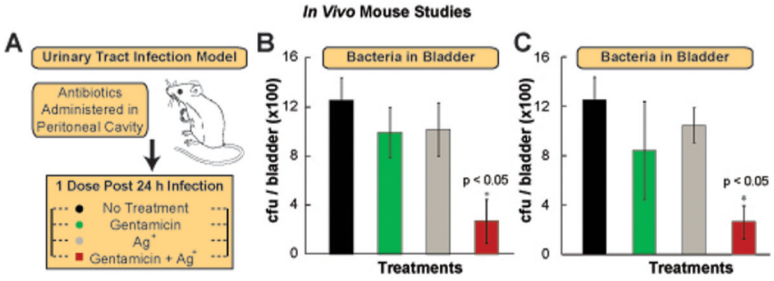

Fig. 6. Ag^+ potentiates bactericidal antibiotic activity *in vivo* in a urinary tract mouse infection model

(A) Schematic of the experimental protocol for the urinary tract infection mouse model. **(B)** CFU of wildtype *E. coli* found in the bladder of infected mice 24 h after no treatment or treatment with 1.25 mg gentamicin/kg body weight, 6 mg $AgNO_3$/kg body weight (35 μM), and 1.25 mg gentamicin/kg body weight in combination with 6 mg $AgNO_3$/kg body weight. **(C)** CFU of wildtype *E. coli* found in the bladder of mice after 24 h treatment with: no treatment, 2.5 mg gentamicin/kg body weight, 3 mg $AgNO_3$/kg body weight (15 μM), and 2.5 mg gentamicin/kg body weight in combination with 3 mg $AgNO_3$/kg body weight. Error bars represent mean ± SEM for at least 6 biological replicates. *** indicates a p-value of <0.001 and ** indicates a p-value of <0.05 as determined by a student t-test, indicating a significant difference from the untreated control, unless otherwise indicated.

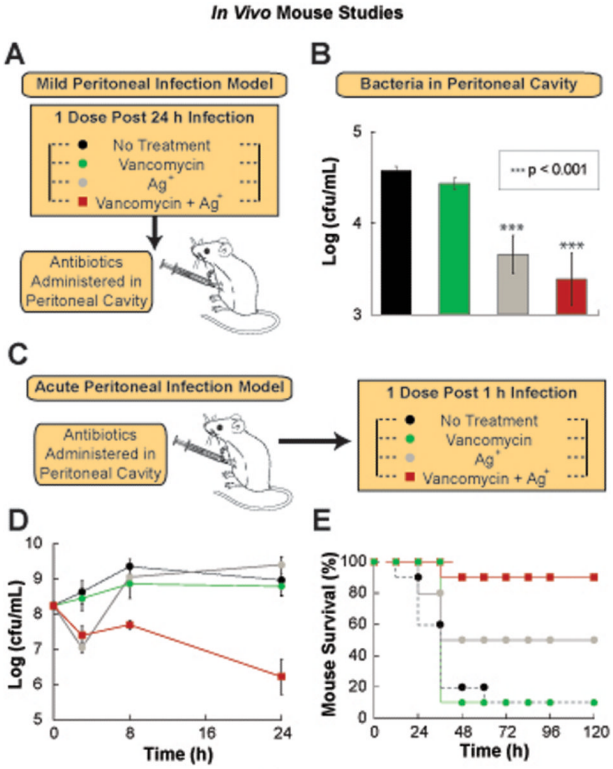

Fig. 7. Ag^+ potentiates vancomycin activity in a mouse peritonitis infection model

(A) Schematic of the experimental protocol for the mild peritonitis mouse model. **(B)** Kill curves of wildtype *E. coli* within the peritoneal cavity of mice after no treatment or treatment with 30 mg vancomycin/kg body weight, 6 mg $AgNO_3$/kg body weight (35 μM), and 30 mg vancomycin/kg body weight in combination with 6 mg $AgNO_3$/kg body weight. **(C)** Schematic of the experimental protocol for the acute mouse models of peritonitis. **(D)** Kill curves of wildtype *E. coli* within the peritoneal cavity of mice after no treatment or treatment with 30 mg vancomycin/kg body weight, 6 mg $AgNO_3$/kg body weight (35 μM), and 30 mg vancomycin/kg body weight in combination with 6 mg $AgNO_3$/kg body weight. **(E)** Survival of mice, with an acute intraperitoneal infection induced with an initial inoculum of 5×10^6 wildtype *E. coli*, after no treatment or treatment with30 mg vancomycin/kg body weight, 6 mg $AgNO_3$/kg body weight (35 μM), and 30 mg vancomycin/kg body weight in combination with 6 mg $AgNO_3$/kg body weight. Error bars represent mean ± SEM for at least 6 biological replicates. ** indicates a p-value of <0.05 as determined by a student t-test, indicating a significant difference from the untreated control. 10 mice per treatment group were used for the survival studies.

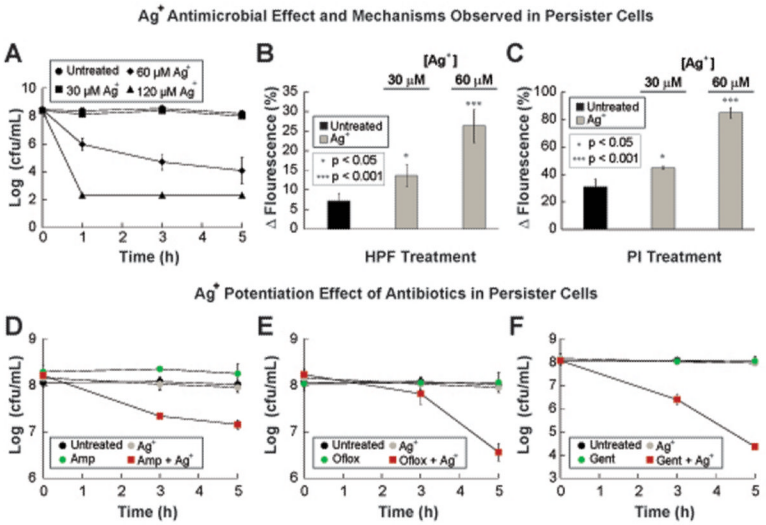

Fig. 8. Ag^+ potentiates bactericidal antibiotic activity *in vitro* against bacterial persister cells

(A) Kill curves for persister *E. coli* cells treated with various concentrations of $AgNO_3$. **(B)** Changes in HPF fluorescence after 3 h of administering $AgNO_3$ at various concentrations. ($p<0.05$ and 0.001 for 30 and 60 μM, respectively) **(C)** Changes in PI fluorescence after 3 h of administering different concentrations of $AgNO_3$. ($p<0.05$ and 0.001 for 30 and 60 μM, respectively) **(D, E)** Kill curves for *E. coli* persister cells treated with 30 μM $AgNO_3$, 5 μg/mL gentamicin (Gent), 3 μg/mL ofloxacin (Oflox), 10 μg/mL ampicillin (Amp), and combinations of $AgNO_3$ with the respective antibiotics. Error bars represent mean ± SEM for at least 6 biological replicates. *** indicates a p-value of <0.001 and ** indicates a p-value of <0.05 as determined by a student t-test, indicating a significant difference from the untreated control, unless otherwise indicated.

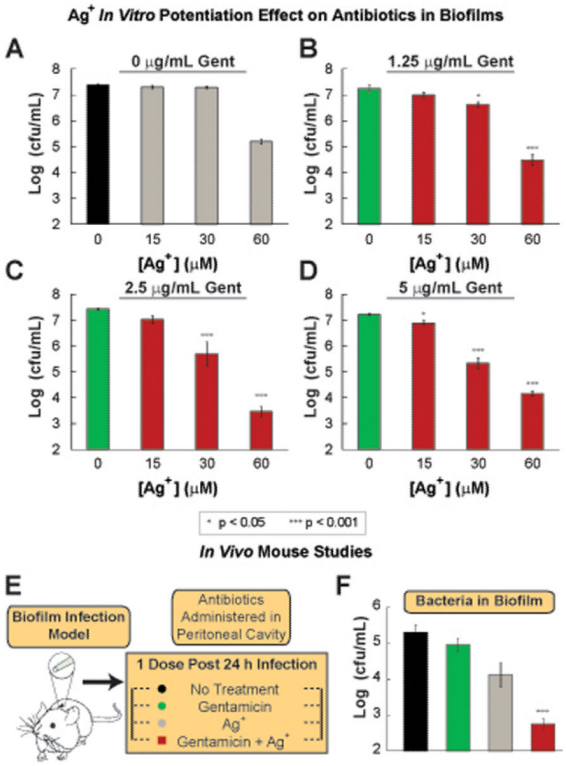

Fig. 9. Ag^+ potentiates bactericidal antibiotics against biofilms both *in vitro* and *in vivo*

(A)–(D) Log (cfu/mL) of *E. coli* within biofilms after treatment for 5 h with combinations of various $AgNO_3$ concentrations, and **(A)** 0, **(B)** 1.25, **(C)** 2.5 and **(D)** 5 μg/mL gentamicin (Gent). **(E)** Schematic of the *in vivo* biofilm infection model. **(F)** CFU of wildtype *E. coli* found in the disrupted biofilm from the catheter 24 h after treatment with: no treatment, 2.5 mg gentamicin/kg body weight, 6 mg $AgNO_3$/kg body weight (35 μM), and 2.5 mg gentamicin/kg body weight in combination with 6 mg $AgNO_3$/kg body weight. Error bars represent mean ± SEM for at least 6 biological replicates. *** indicates a p-value of <0.001 and ** indicates a p-value of <0.05 as determined by a student t-test, indicating a significant difference from the untreated control, unless otherwise indicated.